Journal of Photochemistry and Photobiology A: Chemistry 205 (2009) 215–220

Contents lists available at ScienceDirect

Journal of Photochemistry and Photobiology A: Chemistry

journal homepage: www.elsevier.com/locate/jphotochem

Effects of alkyl chain length on Cu(II)-selective green fluorescence of rhodamine–diacetic acid conjugates

Xuan Zhang [1], Shigehiro Sumiya, Yasuhiro Shiraishi *, Takayuki Hirai

Research Center for Solar Energy Chemistry, and Division of Chemical Engineering, Graduate School of Engineering Science, Osaka University, Toyonaka 560-8531, Japan

ARTICLE INFO

Article history:
Received 31 January 2009
Received in revised form 19 March 2009
Accepted 4 May 2009
Available online 18 May 2009

Keywords:
Rhodamine
Fluorescent chemosensor
Self-assembly
Copper
Mercury

ABSTRACT

Fluorescence properties of rhodamine–diacetic acid conjugates (**1a–e**), with different alkyl chain length (C2–C6) between the rhodamine and the diacetic acid moieties, have been studied in the presence of Cu^{2+} and Hg^{2+}. Without cations or with other cations, these probes show almost no fluorescence; however, addition of Cu^{2+} creates strong green fluorescence at around 530 nm, while Hg^{2+} addition shows weak orange fluorescence at around 580 nm. The Cu^{2+}-induced green fluorescence originates from self-assembled aggregates of the probes formed by coordination association with multiple Cu^{2+} ions. Coordination association of the probes with Cu^{2+} is weakened with an increase in the chain length of the probes due to longer distance between the amide oxygen and the diacetic acid binding sites. In contrast, the green fluorescence intensity is not related to the coordination association strength; some probes show high fluorescence intensity. This is probably because alkyl chains sterically affect the alignment of the probes during aggregation interaction and, hence, produces aggregates with different fluorescence property.

1. Introduction

Rhodamine is a dye used extensively as a fluorescent labeling reagent and a dye laser source because of excellent photophysical properties, such as long absorption and emission wavelengths, high fluorescence quantum yield, and large absorption coefficient [1]. Recently, various kinds of rhodamine-based fluorescent probes have been proposed for selective detection of metal cations, such as Pb^{2+} [2], Cu^{2+} [3,4], Hg^{2+} [5,6], and Fe^{3+} [7]. The cation sensing mechanism of these probes is based on the structural change of the rhodamine moiety from spirocyclic form to open-ring form. Without cations, these probes exist in spirocyclic form, colorless and nonfluorescent. Addition of targeted metal cation leads to spirocycle opening via reversible coordination [2,3,5,7] or irreversible chemical reaction with the ligand moiety [4,6], resulting in an appearance of pink color (556 nm absorption) and orange fluorescence (580 nm).

In a previous work [8], we synthesized a novel rhodamine derivative (Scheme 1, **1a**) containing an ethylenediamine-*N*,*N*-diacetic acid moiety, an analogue of classic chelator of EDTA. The probe, **1a**, shows Cu^{2+}-selective "green" fluorescence at 530 nm in acetonitrile (CH_3CN). In contrast, addition of Hg^{2+} shows weak ordinary orange fluorescence at 580 nm, and other cations do not show any fluorescence. This is the first rhodamine-based fluorescent probe exhibiting metal-induced green fluorescence, whereas all of the early-reported rhodamine-based probes show orange fluorescence [2–7]. Our experimental findings reveal that the Cu^{2+}-selective green fluorescence of **1a** is due to the direct photoexcitation of a self-assembled aggregate of multiple **1a** molecules formed by coordination association with multiple Cu^{2+} ions. However, the detailed property of the green emitting aggregate is still unclear.

In the present work, we synthesized a series of rhodamine–diacetic acid conjugates with different alkyl chain length of the diamine moiety varying from C3 to C6 (Scheme 1, **1b–e**). Fluorescence behaviors of these probes against Cu^{2+} and Hg^{2+} have been studied in comparison to that of **1a** to clarify how the alkyl chain length affects the Cu^{2+}-selective green fluorescence. All of these probes show Cu^{2+}-selective green fluorescence, while showing very weak orange fluorescence against Hg^{2+}. However, the coordination and aggregation behaviors and fluorescence properties of these probes are strongly affected by the alkyl chain length.

2. Experimental

2.1. Materials

All of the reagents were purchased from Tokyo Kasei and used without further purification. Perchlorate salts of Cu^{2+} and Hg^{2+}

* Corresponding author. Tel.: +81 6 6850 6271; fax: +81 6 6850 6273.
E-mail address: shiraish@cheng.es.osaka-u.ac.jp (Y. Shiraishi).
[1] Present address: Macromolecules Group, Organic Nanomaterials Center, National Institute for Materials Science (NIMS), Tsukuba, 305-0047, Japan.

1010-6030/$ – see front matter © 2009 Elsevier B.V. All rights reserved.
doi:10.1016/j.jphotochem.2009.05.006

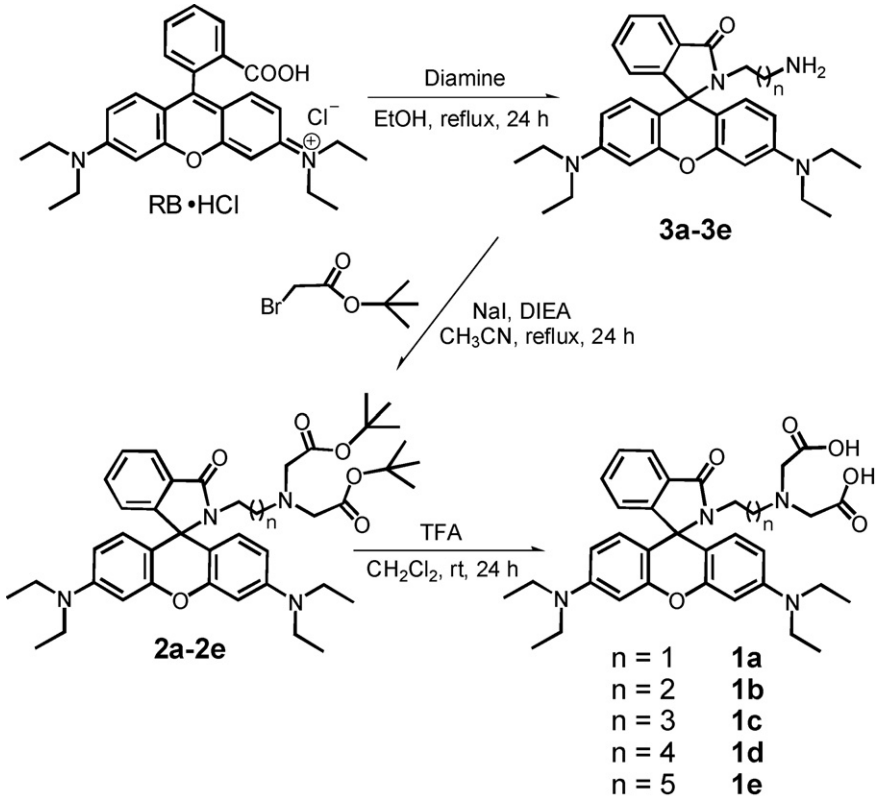

Scheme 1. Synthesis of **1a**–**e**.

were used as the metal source. The rhodamine–diacetic acid conjugates, **1b**–**e**, were synthesized according to procedure similar to that for **1a** [8], as summarized in Scheme 1 and as below. ^{1}H, ^{13}C NMR, and FAB-MS charts of the respective materials are summarized in Supplementary Material (Figs. S6–S41).

*2.1.1. Synthesis of **3b**–**e***

Rhodamine B hydrochloride (1.20 g, 2.5 mmol) was dissolved in ethanol (30 mL). Excess amount of respective diamines (2 mL) was added dropwise to the solution and refluxed for 24 h. The solution was concentrated by evaporation. Water (20 mL) was added to the resultant and extracted with CH_2Cl_2 (20 mL × 2). The combined organic phase was washed twice with water and dried over Na_2SO_4. The solvent was removed by evaporation and dried in vacuo, affording pale-pink solids of **3b**–**e**.

3b. Yield 70%. ^{1}H NMR (270 MHz, $CDCl_3$): δ (ppm) = 7.86–7.83 (m, 1H), 7.50–7.43 (m, 2H), 7.14–7.09 (m, 1H), 6.36–6.20 (m, 6H), 3.35–3.22 (m, 10H), 2.71 (t, J = 5.4 Hz, 2H), 1.34 (t, J = 5.4 Hz, 2H), 1.14 (t, J = 6.7 Hz, 12H). ^{13}C NMR (67.8 MHz, $CDCl_3$): δ (ppm) = 169.02, 153.20, 153.00, 148.82, 132.69, 130.48, 128.22, 123.72, 122.85, 108.13, 104.67, 97.67, 65.58, 44.35, 36.89, 35.62, 26.62, 12.59. MS (FAB): anal. calcd for $C_{31}H_{38}N_4O_2$: 498.6; found: 499.2 (M+H$^+$, 100%).

3c. Yield 69%. ^{1}H NMR (270 MHz, $CDCl_3$): δ (ppm) = 7.90–7.85 (m, 1H), 7.44–7.37 (m, 2H), 7.07–7.02 (m, 1H), 6.43–6.22 (m, 6H), 3.32 (q, J = 6.7 Hz, 8H), 3.10 (t, J = 8.1 Hz, 2H), 2.44 (t, J = 6.7 Hz, 2H), 1.27–1.12 (m, 16H). ^{13}C NMR (67.8 MHz, $CDCl_3$): δ (ppm) = 167.68, 153.15, 148.52, 131.96, 131.38, 128.78, 127.74, 123.54, 122.46, 107.86, 105.87, 97.62, 64.77, 44.31, 41.59, 39.90, 31.21, 25.38, 12.60. MS (FAB): anal. calcd for $C_{32}H_{40}N_4O_2$: 512.6; found: 513.3 (M+H$^+$, 100%).

3d. Yield 65%. ^{1}H NMR (270 MHz, $CDCl_3$): δ (ppm) = 7.82–7.79 (m, 1H), 7.37–7.31 (m, 2H), 7.01–6.96 (m, 1H), 6.36–6.13 (m, 6H), 3.26 (q, J = 6.7 Hz, 8H), 3.03 (t, J = 6.7 Hz, 2H), 2.48 (t, J = 6.7 Hz, 2H), 2.22 (br, 2H, NH), 1.22–1.06 (m, 18H). ^{13}C NMR (67.8 MHz, $CDCl_3$): δ (ppm) = 167.75, 153.22, 153.06, 148.48, 131.94, 131.20, 128.67, 127.70, 123.47, 122.42, 107.86, 105.70, 97.58, 64.86, 44.26, 41.14, 40.03, 31.42, 27.81, 24.14, 12.56. MS (FAB): anal. calcd for $C_{33}H_{42}N_4O_2$: 526.6; found: 527.3 (M+H$^+$, 100%).

3e. Yield 60%. ^{1}H NMR (270 MHz, $CDCl_3$): δ (ppm) = 7.90–7.85 (m, 1H), 7.42–7.37 (m, 2H), 7.07–7.01 (m, 1H), 6.42–6.16 (m, 6H), 3.32 (q, J = 6.7 Hz, 8H), 3.07 (t, J = 6.7 Hz, 2H), 2.53 (t, J = 6.7 Hz, 2H), 1.47 (br, 2H, NH), 1.23–1.08 (m, 20H). ^{13}C NMR (67.8 MHz, $CDCl_3$): δ (ppm) = 167.66, 153.25, 153.09, 148.47, 131.88, 131.35, 128.76, 127.67, 123.49, 122.42, 107.86, 105.91, 97.60, 64.75, 44.28, 41.94, 40.15, 33.29, 28.00, 26.73, 26.15, 12.59. MS (FAB): anal. calcd for $C_{34}H_{44}N_4O_2$: 540.6; found: 541.3 (M+H$^+$, 100%).

*2.1.2. Synthesis of **2b**–**e***

3b–**e** (1 mmol) was dissolved in a mixture of CH_3CN (10 mL) and DMSO (10 mL). NaI (0.30 g, 2 mmol), *N*,*N*-diisopropylethylamine (2 mL, 12 mmol), and *tert*-butyl bromoacetate (0.45 mL, 3 mmol) were added to the mixture and refluxed for 24 h under dry N_2. The solution was concentrated by evaporation. Water (20 mL) was added to the residue and extracted with CH_2Cl_2 (20 mL × 2). The combined organic phase was washed twice with water, dried over Na_2SO_4, and concentrated by evaporation. The resultant was purified by a column chromatography (silica gel, ethyl acetate/hexane = 1/1, v/v), affording light-yellow semi-solids of **2b**–**e**.

2b. Yield 63%. ^{1}H NMR (270 MHz, $CDCl_3$): δ (ppm) = 7.83–7.79 (m, 1H), 7.36–7.30 (m, 2H), 7.00–6.96 (m, 1H), 6.37–6.17 (m, 6H), 3.30–3.05 (m, 14H), 2.46 (t, J = 6.7 Hz, 2H), 1.43–1.29 (m, 20H), 1.09 (t, J = 6.7 Hz, 12H). ^{13}C NMR (67.8 MHz, $CDCl_3$): δ (ppm) = 170.23, 167.56, 153.38, 153.09, 148.48, 131.85, 131.47, 128.67, 127.62, 123.48,

122.36, 107.92, 105.79, 97.68, 80.44, 64.77, 55.19, 51.75, 44.26, 38.36, 28.11, 26.15, 12.63. MS (FAB): anal. calcd for $C_{43}H_{58}N_4O_6$: 726.9; found: 727.4 ($M+H^+$, 100%).

2c. Yield 60%. ^{1}H NMR (270 MHz, $CDCl_3$): δ (ppm) = 7.89–7.84 (m, 1H), 7.40–7.36 (m, 2H), 7.05–7.02 (m, 1H), 6.42–6.22 (m, 6H), 3.36–3.06 (m, 14H), 2.44 (t, J = 8.1 Hz, 2H), 1.40–1.12 (m, 34H). ^{13}C NMR (67.8 MHz, $CDCl_3$): δ (ppm) = 170.44, 167.73, 153.39, 153.11, 148.54, 131.90, 131.36, 128.73, 127.70, 123.58, 122.44, 107.94, 105.98, 97.73, 80.52, 64.79, 55.64, 53.97, 44.32, 40.24, 28.17, 26.01, 25.58, 12.66. MS (FAB): anal. calcd for $C_{44}H_{60}N_4O_6$: 740.9; found: 741.3 ($M+H^+$, 100%).

2d. Yield 60%. ^{1}H NMR (270 MHz, $CDCl_3$): δ (ppm) = 7.88–7.85 (m, 1H), 7.40–7.37 (m, 2H), 7.05–7.02 (m, 1H), 6.42–6.22 (m, 6H), 3.36–3.04 (m, 14H), 2.49 (t, J = 8.1 Hz, 2H), 1.49–1.08 (m, 36H). ^{13}C NMR (67.8 MHz, $CDCl_3$): δ (ppm) = 170.36, 167.64, 153.36, 153.05, 148.48, 131.81, 131.45, 128.66, 127.59, 123.45, 122.39, 107.85, 105.87, 97.66, 80.47, 64.73, 55.66, 54.18, 44.26, 40.30, 28.11, 28.03, 27.52, 24.89, 12.60. MS (FAB): anal. calcd for $C_{45}H_{62}N_4O_6$: 754.9; found: 755.4 ($M+H^+$, 70%).

2e. Yield 60%. ^{1}H NMR (270 MHz, $CDCl_3$): δ (ppm) = 7.88–7.85 (m, 1H), 7.40–7.37 (m, 2H), 7.05–7.02 (m, 1H), 6.42–6.22 (m, 6H), 3.35–3.04 (m, 14H), 2.55 (t, J = 8.1 Hz, 2H), 1.50–1.07 (m, 38H). ^{13}C NMR (67.8 MHz, $CDCl_3$): δ (ppm) = 170.24, 167.49, 153.25, 152.97, 148.36, 131.72, 131.23, 128.59, 127.51, 123.36, 122.28, 107.77, 105.90, 97.57, 80.37, 64.61, 55.62, 54.00, 44.17, 40.30, 28.02, 27.67, 27.49, 27.00, 26.66, 12.50. MS (FAB): anal. calcd for $C_{46}H_{64}N_4O_6$: 768.9; found: 769.4 ($M+H^+$, 60%)

2.1.3. Synthesis of ***1b–e***

2b–e (0.5 mmol) was dissolved in CH_2Cl_2 (2 mL). Trifluoroacetic acid (2 mL) was added dropwise to the solution and stirred at room temperature for 24 h. The solution was concentrated by evaporation. The residue was washed twice with diethyl ether and dried in vacuo, affording purple powders of **1b–e**.

1b. Yield 99%. ^{1}H NMR (270 MHz, $CDCl_3$): δ (ppm) = 11.65 (br, 2H), 7.96–6.53 (m, 10H), 3.90–3.23 (m, 16H), 1.42–1.13 (m, 14H). ^{13}C NMR (100.4 MHz, $CDCl_3$): δ (ppm) = 169.11, 167.96, 161.81, 161.46, 161.10, 157.50, 155.06, 152.54, 145.01, 133.20, 129.76, 129.05, 123.26, 117.73, 114.82, 111.93, 104.01, 64.97, 55.36, 54.23, 47.90, 36.76, 27.85, 23.87, 15.23, 12.49, 11.56. MS (FAB): anal. calcd for $C_{35}H_{42}N_4O_6$: 614.7; found: 615.3 ($M+H^+$, 100%).

1c. Yield 99%. ^{1}H NMR (270 MHz, $CDCl_3$): δ (ppm) = 12.00 (br, 2H), 7.84–6.53 (m, 10H), 4.01–3.05 (m, 16H), 1.53–0.99 (m, 16H). ^{13}C NMR (100.4 MHz, $CDCl_3$): δ (ppm) = 168.51, 167.95, 161.14, 160.92, 152.50, 145.04, 133.18, 130.00, 129.16, 123.02, 118.43, 114.13, 111.92, 103.64, 64.72, 55.04, 47.84, 38.74, 15.22, 12.47, 11.62. MS (FAB): anal. calcd for $C_{36}H_{44}N_4O_6$: 628.7; found: 629.3 ($M+H^+$, 100%)

1d. Yield 99%. ^{1}H NMR (270 MHz, $CDCl_3$): δ (ppm) = 11.17 (br, 2H), 7.85–6.54 (m, 10H), 4.03–3.12 (m, 16H), 1.51–1.13 (m, 18H). ^{13}C NMR (100.4 MHz, $CDCl_3$): δ (ppm) = 168.23, 168.09, 161.91, 161.56, 161.20, 152.57, 152.49, 144.73, 132.81, 130.52, 129.37, 128.62, 123.57, 122.92, 117.79, 114.88, 111.99, 103.69, 64.65, 56.11, 55.23, 47.98, 39.61, 27.67, 23.59, 12.47, 11.59. MS (FAB): anal. calcd for $C_{37}H_{46}N_4O_6$: 642.7; found: 643.3 ($M+H^+$, 100%)

1e. Yield 99%. ^{1}H NMR (270 MHz, $CDCl_3$): δ (ppm) = 11.88 (br, 2H), 7.88–6.43 (m, 10H), 4.09–3.14 (m, 16H), 1.57–1.14 (m, 20H). ^{13}C NMR (100.4 MHz, $CDCl_3$): δ (ppm) = 168.24, 167.92, 161.75, 161.39, 161.03, 160.71, 152.36, 142.96, 130.44, 129.81, 123.51, 117.63, 114.73, 113.88, 112.01, 106.31, 64.41, 55.05, 49.62, 27.74, 26.29, 12.46, 11.15. MS (FAB): anal. calcd for $C_{38}H_{48}N_4O_6$: 656.7; found: 657.3 ($M+H^+$, 100%)

2.2. Analysis

Fluorescence spectra were recorded on a Hitachi F-4500 Fluorescence Spectrometer. Absorption spectra were measured on a Multispec-1500 spectrophotometer (Shimadzu). The measurements were carried out with 1-cm path length quartz cell. The spectra were measured after mixing the probe solution and metal cations for 8 h at the designated temperature (293 K, unless otherwise noted). ^{1}H and ^{13}C NMR spectra were recorded on JEOL JNM-GSX270 Excalibur. FAB-MS spectra were obtained from JEOL JMS 700 Mass spectrometer. Fluorescence quantum yield was measured with fluorescein as standard (Φ_F = 0.85 in 0.1 M NaOH) [9].

3. Results and discussion

3.1. Spectroscopic behavior

Fig. 1 shows fluorescence spectra (λ_{ex} = 480 nm) of the respective **1a–e** probes (25 μM) measured in CH_3CN at 293 K. Without metal cation, all these probes show almost no fluorescence at around 575 nm, as is the case for **1a** (Fig. 1a) [8]. Addition of Cu^{2+}, however, creates strong and blue-shifted fluorescence at 530 nm ("green" fluorescence). It must be noted that, as shown in Figs. S1–S5 (Supplementary Material), addition of Hg^{2+} to all of the probes shows only a weak fluorescence at 575 nm ("orange" fluorescence), as is the case for **1a** [8]. In contrast, addition of other metal cations (Pb^{2+}, Zn^{2+}, Cd^{2+}, Fe^{2+}, Ca^{2+}, Co^{2+}, Mn^{2+}, Fe^{3+}, Ag^+, Li^+, Na^+, K^+) to all of the probes does not show fluorescence. These findings indicate that **1a–e** probes show similar fluorescence behaviors against metal cations.

As shown in Fig. 1, addition of <2 equiv of Cu^{2+} to all of the probes leads to increase in the 575 nm emission; however, addition of >2 equiv of Cu^{2+} leads to blue-shift of the emission band, along with an increase in the emission intensity. Accordingly, the fluorescence color of the solution changes continuously from orange to green. As shown in Fig. 1 (inset), the emission intensity for all of the probes monitored at 530 nm increases with an increase in the Cu^{2+} amount up to 5–6 equiv, but decreases upon further Cu^{2+} addition. These fluorescence behaviors of **1b–e** are similar to that of **1a** (Fig. 1a) [8]. The fluorescence quantum yields of **1a–e** measured with 5 equiv of Cu^{2+} are also similar (0.32, 0.37, 0.31, 0.38, and 0.30, respectively). The fluorescence response of **1b–e** to Hg^{2+} is also similar to that of **1a**; as shown in Figs. S1–S5 (Supplementary Material), Hg^{2+} addition to all of the probes leads to monotonous increase in the 580 nm emission, where blue-shift of the emission does not occur [8].

Fig. 2 shows change in absorption spectra of **1a–e**. Without cations, these show weak absorption at 500–600 nm, indicating that these exist as spirocycle-closed forms [2–7]. This is confirmed by ^{13}C NMR analysis (Supplementary Material; Figs. S31, S34, S37, and S40); **1a–e** probes show distinctive chemical shifts at 65.84, 64.97, 64.72, 64.65, 64.41 ppm, respectively, which are assigned to the closed spirocycle carbons [8]. As shown in Fig. 2, addition of <2 equiv of Cu^{2+} to **1a–e** probes leads to increase in 556 nm absorption; however, upon addition of >2 equiv of Cu^{2+}, the 556 nm absorption decreases and 506 nm absorption appears. However, as shown in inset, the 506 nm absorbance decreases with an addition of about >4 equiv of Cu^{2+}. These absorption behaviors are similar to that of **1a** [8], and the appearance of the 506 nm absorption is consistent with the blue-shift of the emission band (Fig. 1). Absorption response of **1b–e** to Hg^{2+} is also similar to that of **1a** [8]; as shown in Figs. S1–S5 (Supplementary Material), addition of Hg^{2+} to **1a–e** leads to monotonous increase in the 556 nm absorbance, where blue-shift of the absorption band does not occur.

Fluorescence excitation spectra of **1a–e** monitored at 580 nm with Hg^{2+} appear at 559 nm, which are similar to the absorption spectra (Figs. S1–S5, Supplementary Material). In contrast, as shown in Fig. 3, Cu^{2+} addition to **1a–e** shows different behavior. With <2 equiv of Cu^{2+}, excitation band similar to that obtained with

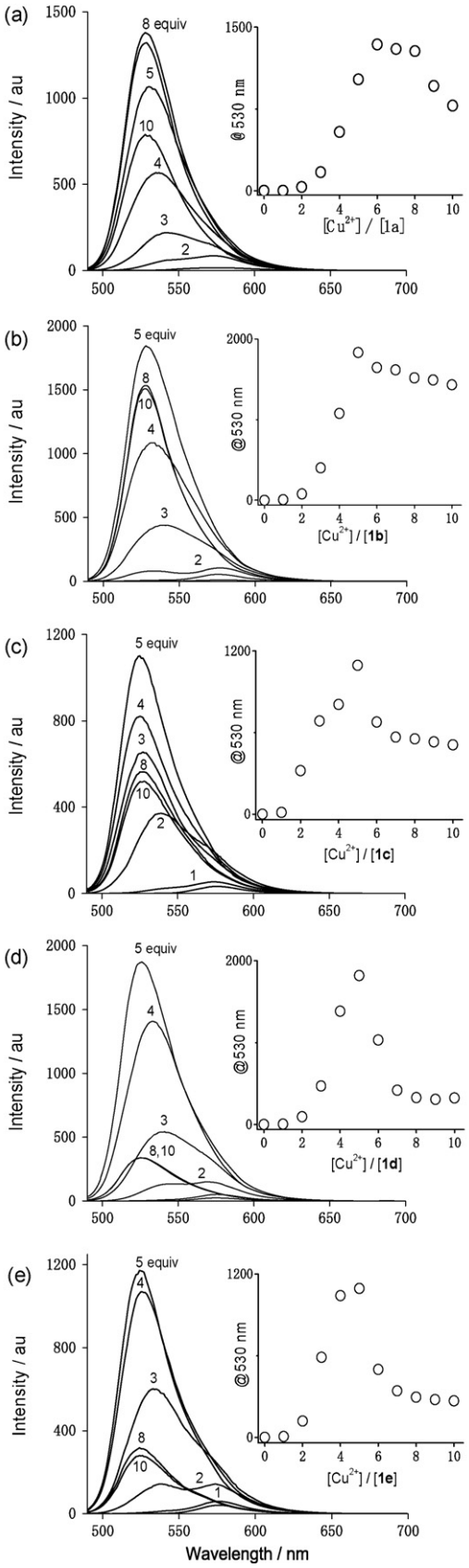

Fig. 1. Fluorescence titration results (λ_{ex} = 480 nm) of (a) **1a**, (b) **1b**, (c) **1c**, (d) **1d**, and (e) **1e** (25 μM) with Cu^{2+} in CH_3CN. (Inset) change in fluorescence intensity monitored at 530 nm.

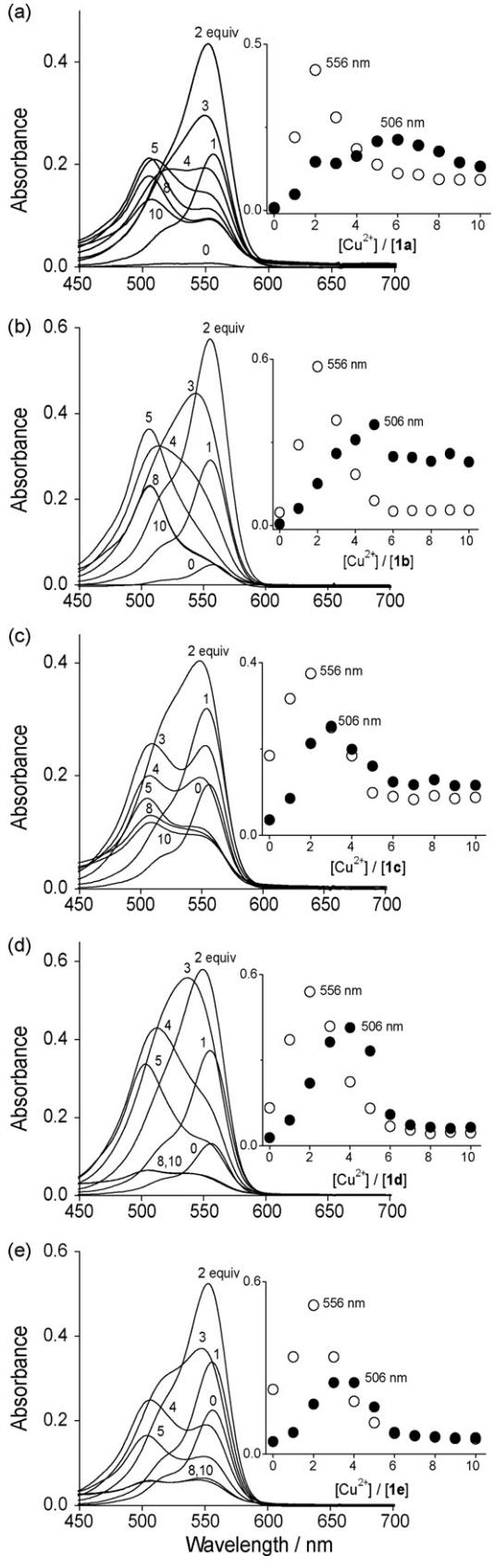

Fig. 2. Absorption titration results of (a) **1a**, (b) **1b**, (c) **1c**, (d) **1d**, and (e) **1e** (25 μM) with Cu^{2+} in CH_3CN. (Inset) change in absorbance at 556 and 506 nm.

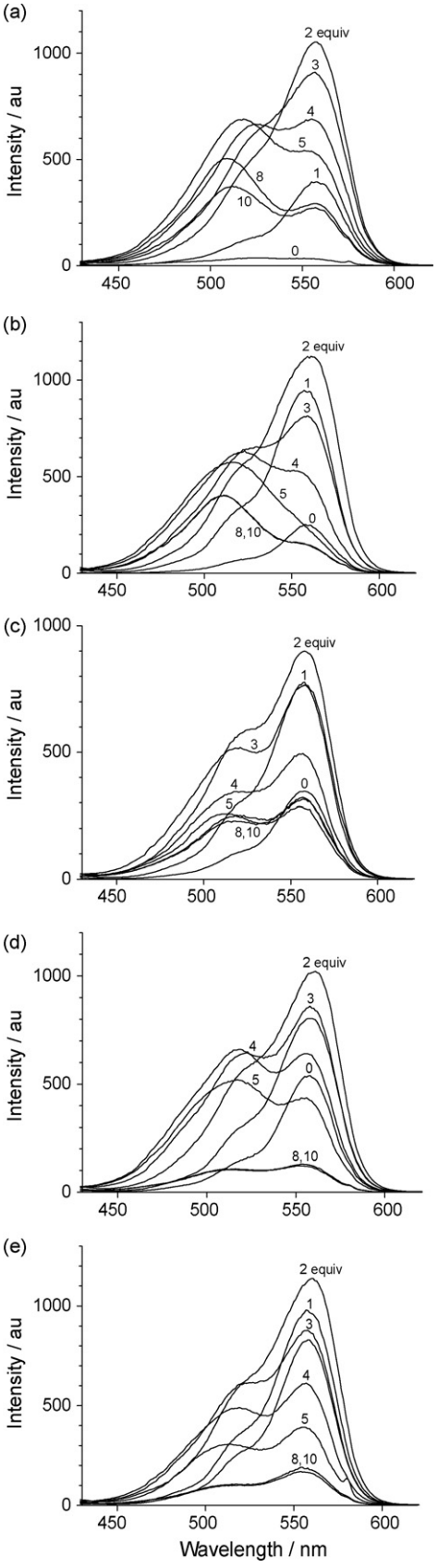

Fig. 3. Fluorescence excitation spectra of (a) **1a**, (b) **1b**, (c) **1c**, (d) **1d**, and (e) **1e** (25 μM) monitored at λ_{em} = 580 nm with Cu^{2+} in CH_3CN.

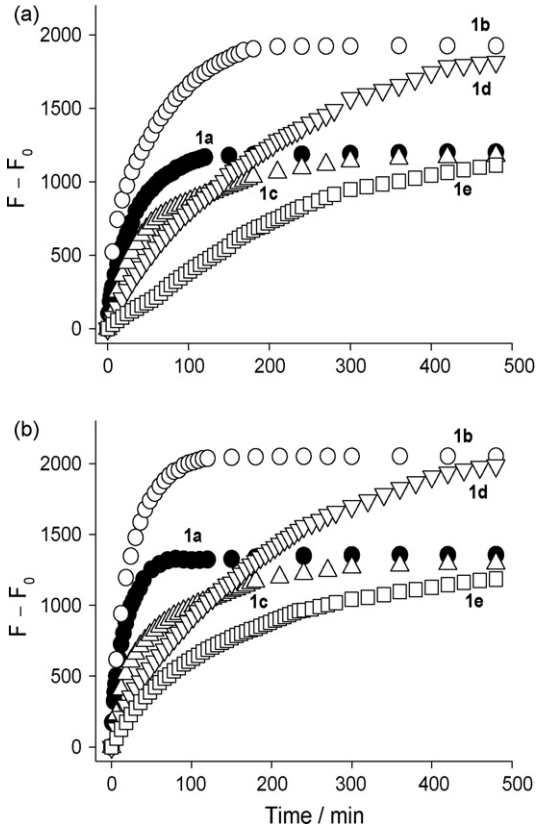

Fig. 4. Time-dependent change in the fluorescence intensity of **1a**–**e** (25 μM) in CH_3CN measured after addition of 5 equiv of Cu^{2+} at (a) 293 and (b) 303 K (λ_{ex} = 480 nm, λ_{em} = 530 nm).

Hg^{2+} appears at 559 nm. However, with >2 equiv of Cu^{2+}, the 559 nm band decreases and a blue-shifted band appears at 450–550 nm. These spectral changes are quite similar to the change in absorption spectra (Fig. 2). These data clearly suggest that, as is the case for **1a** [8], the green fluorescence of **1b**–**e** obtained with Cu^{2+} is due to direct photoexcitation of the self-assembled aggregates of the probes formed by coordination association with multiple Cu^{2+} ions.

3.2. Properties of green fluorescence

Fig. 4a shows time-dependent change in the green fluorescence intensity (530 nm) of **1a**–**e** measured after addition of 5 equiv of Cu^{2+} at 293 K. Saturation of the emission increase requires more than 100 min. In contrast, as shown in Fig. 5, Hg^{2+} addition to **1a**–**e** allows rapid saturation of the 580 nm emission (<100 min). This indicates that, as described for **1a** [8], Cu^{2+}-induced formation of the green emitting aggregates of **1a**–**e** requires aggregation interaction of the probe molecules. As is usually observed for related rhodamine-based probes [2–7], the Hg^{2+}-induced orange fluorescence of **1a**–**e** is explained by spirocycle-opening mechanism; coordination of the amide oxygen of the probes with Hg^{2+} leads to spirocycle-opening, leading to an appearance of orange fluorescence. In contrast, formation of the green emitting aggregate requires aggregation interaction of the probes in addition to the spirocycle-opening. This therefore requires longer saturation time for emission increase (Fig. 4a). As reported [10], rhodamine aggregation is accelerated at higher temperature due to the decrease in solvation interaction. As shown in Fig. 4b, at higher temperature (303 K), the green emission of **1a**–**e** after Cu^{2+} addition indeed saturates more rapidly. This clearly indicates that aggregation inter-

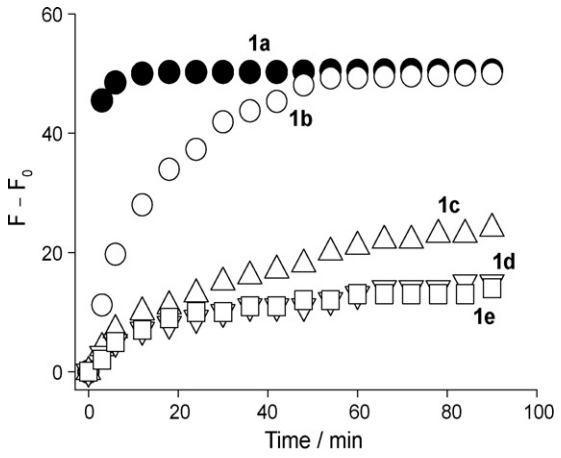

Fig. 5. Time-dependent change in the fluorescence intensity of **1a**–**e** (25 μM) in CH_3CN measured after addition of 5 equiv of Hg^{2+} at 293 K (λ_{ex} = 480 nm, λ_{em} = 580 nm).

action is actually involved for the formation of green emitting species. In addition, Cu^{2+}-induced blue shift of the absorption spectra (Fig. 2) indicates that these aggregates probably have a face-to-face (sandwich) structure (H-type aggregate) [11].

Besides the similar fluorescence and absorption behaviors of **1a**–**e**, some different features are observed. In the case with Hg^{2+}, as shown in Fig. 5, saturation time of the orange fluorescence becomes longer with an increase in the chain length (**1a** < **1b** < **1c** < **1d**, **1e**). In addition, the fluorescence enhancement decreases with an increase in the chain length (**1a**, **1b** < **1c** < **1d**, **1e**). These may be because the coordination interaction between the amide oxygen of the probes and Hg^{2+} is weakened with an increase in the alkyl chain length. This can be rationalized from the increased distance between the coordination sites (amide oxygen and carboxylic acid moieties). The insufficient interaction between the amide oxygen and Hg^{2+} probably results in longer saturation time and smaller enhancement of the orange fluorescence.

Effect of alkyl chain length on the fluorescence response of **1a**–**e** to Cu^{2+} is more complicated. As shown in Fig. 4, saturation time of the green fluorescence becomes longer with an increase in the chain length (**1a** < **1b** < **1c** < **1d**, **1e**). This may be due to the weakened binding interaction between the amide oxygen and Cu^{2+}, as is the case for Hg^{2+}. In contrast, as shown in Fig. 4, the green fluorescence enhancement of **1b** and **1d** is much higher than that of **1a**, whereas the intensities of **1c** and **1e** are comparable to that of **1a**. This suggests that green emitting aggregates of **1b** and **1d** have a more fluorescent structure. As reported [12], fluorescence intensity of H-aggregates strongly depends on the distance and orientation of the dye molecules. Detailed aggregation mechanism of **1b** and **1d** containing multiple Cu^{2+} ions cannot be clarified at this stage. However, the above findings imply that, during aggregation interaction of the probes, alkyl chains may sterically affect the alignment of the probes. As a result of this, the **1b** and **1d** probes with C3 and C5 alkyl chain may provide better geometry for the aggregation, probably resulting in the formation of more fluorescent aggregate.

4. Conclusion

Fluorescence properties of rhodamine–diacetic acid conjugates (**1a**–**e**) with different alkyl chain length between the rhodamine and the diacetic acid moieties, have been studied in the presence of Cu^{2+}. All of these probes show Cu^{2+}-selective green fluorescence, which originates from aggregates of the probes formed by coordination association with multiple Cu^{2+} ions. With an increase in the alkyl chain length, coordination association of the probes with Cu^{2+} is weakened because of the longer distance between the binding sites. In contrast, the green fluorescence intensity for **1b** and **1d** probes is much higher than that of **1a**. This is probably because the alkyl chains affect significantly the alignment of the probes during the aggregation interaction; the **1b** and **1d** probes provide better geometry for aggregation and produce more fluorescent aggregate.

Acknowledgment

This work is supported by Grants-in-Aid for Scientific Research (No. 19760536) from the Ministry of Education, Culture, Sports, Science and Technology, Japan (MEXT).

Appendix A. Supplementary data

Supplementary data associated with this article can be found, in the online version, at doi:10.1016/j.jphotochem.2009.05.006.

References

[1] J.R. Lakowicz, Principles of Fluorescence Spectroscopy, third ed., Springer, New York, 2006, pp. 67–69.
[2] J.Y. Kwon, Y.J. Jang, Y.J. Lee, K.M. Kim, M.S. Seo, W. Nam, J. Yoon, J. Am. Chem. Soc. 127 (2005) 10107–10111.
[3] Y. Xiang, A.-J. Tong, P.-Y. Jin, Y. Ju, Org. Lett. 8 (2006) 2863–2866.
[4] (a) V. Dujols, F. Ford, A.J. Czarnik, J. Am. Chem. Soc. 119 (1997) 7386–7387;
(b) X. Chen, J. Jia, H. Ma, S. Wang, X. Wang, Anal. Chim. Acta 632 (2009) 9–14.
[5] (a) H. Zheng, Z.-H. Qian, L. Xu, F.-F. Yuan, L.-D. Lan, J.-G. Xu, Org. Lett. 8 (2006) 859–861;
(b) M.H. Lee, J.-S. Wu, J.W. Lee, J.H. Jung, J.S. Kim, Org. Lett. 9 (2007) 2501–2504;
(c) D. Wu, W. Huang, C.-Y. Duan, Z.-H. Lin, Q.-J. Meng, Inorg. Chem. 46 (2007) 1538–1540;
(d) J.H. Soh, K.M.K. Swamy, S.K. Kim, S. Kim, S.-H. Lee, J. Yoon, Tetrahedron Lett. 48 (2007) 5966–5969;
(e) H. Yang, Z.-G. Zhou, K.-W. Huang, M.-X. Yu, F.-Y. Li, T. Yi, C.-H. Huang, Org. Lett. 9 (2007) 4729–4732;
(f) W. Shi, H.-M. Ma, Chem. Commun. (2008) 1856–1858;
(g) X.-Q. Zhan, Z.-H. Qian, H. Zheng, B.-Y. Su, Z. Lan, J.-G. Xu, Chem. Commun. (2008) 1859–1861;
(h) Y. Shiraishi, S. Sumiya, Y. Kohno, T. Hirai, J. Org. Chem. 73 (2008) 8571–8574.
[6] (a) Y.-K. Yang, K.-J. Yook, J. Tae, J. Am. Chem. Soc. 127 (2005) 16760–16761;
(b) S.-K. Ko, Y.-K. Yang, J. Tae, I. Shin, J. Am. Chem. Soc. 128 (2006) 14150–14155;
(c) J.-S. Wu, I.-C. Hwang, K.S. Kim, J.S. Kim, Org. Lett. 9 (2007) 907–910.
[7] (a) Y. Xiang, A.-J. Tong, Org. Lett. 8 (2006) 1549–1552;
(b) M. Zhang, Y.-H. Gao, M.-Y. Li, M.-X. Yu, F.-Y. Li, L. Li, M.-W. Zhu, J.-P. Zhang, T. Yi, C.-H. Huang, Tetrahedron Lett. 48 (2007) 3709–3712;
(c) S. Bae, J. Tae, Tetrahedron Lett. 48 (2007) 5389–5392;
(d) X. Zhang, Y. Shiraishi, T. Hirai, Tetrahedron Lett. 48 (2007) 5455–5459;
(e) J. Mao, L.-N. Wang, W. Dou, X.-L. Tang, Y. Yan, W.-S. Liu, Org. Lett. 9 (2007) 4567–4570;
(f) X. Zhang, Y. Shiraishi, T. Hirai, Tetrahedron Lett. 49 (2008) 4178–4181.
[8] X. Zhang, Y. Shiraishi, T. Hirai, Org. Lett. 9 (2007) 5039–5043.
[9] C.A. Parker, W.T. Rees, Analyst 86 (1960) 587–600.
[10] (a) P. Ruiz Ojeda, I.A. Katime Amashta, J. Ramón Ochoa, I. López Arbeloa, J. Chem. Soc. Faraday Trans. 2 (84) (1988) 1–8;
(b) K. Kemnitz, K. Yoshihara, J. Phys. Chem. 95 (1991) 6095–6104.
[11] (a) K.K. Rohatgi, G.S. Singhal, J. Phys. Chem. 70 (1966) 1695–1701;
(b) J.E. Selwyn, J.I. Steinfeld, J. Phys. Chem. 76 (1972) 762–774;
(c) I. López Arbeloa, P. Ruiz Ojeda, Chem. Phys. Lett. 87 (1982) 556–560;
(d) O. Valdes-Aguilera, D.C. Neckers, Acc. Chem. Res. 22 (1989) 171–177.
[12] (a) R.W. Chambers, T. Kajiwara, D.R. Kearns, J. Phys. Chem. 74 (1974) 380–387;
(b) M. Van der Auweraer, G. Biesmans, F.C. De Schryver, Chem. Phys. 119 (1988) 355–375;
(c) A.K. Mandal, M.K. Pal, Chem. Phys. 253 (2000) 115–124;
(d) U. Rösch, S. Yao, R. Wortmann, F. Würthner, Angew. Chem. Int. Ed. 45 (2006) 7026–7030.